Journal of Controlled Release 199 (2015) 63–71

Contents lists available at ScienceDirect

Journal of Controlled Release

journal homepage: www.elsevier.com/locate/jconrel

Detection of hepatocellular carcinoma in transgenic mice by Gd-DTPA- and rhodamine 123-conjugated human serum albumin nanoparticles in T1 magnetic resonance imaging

Waralee Watcharin [a,1], Christian Schmithals [b,1], Thomas Pleli [b], Verena Köberle [b], Hüdayi Korkusuz [c], Frank Hübner [d], Oliver Waidmann [b], Stefan Zeuzem [b], Horst-Werner Korf [e], Andreas Terfort [f], Svetlana Gelperina [g], Thomas J. Vogl [d], Jörg Kreuter [a], Albrecht Piiper [b,*]

[a] Institute for Pharmaceutical Technology, Goethe-University of Frankfurt, Max-von-Laue-Straße 7, D-60438 Frankfurt, Germany
[b] Department of Medicine 1, University Hospital of Frankfurt, Theodor-Stern-Kai 7, D-60590 Frankfurt, Germany
[c] Department of Nuclear Medicine, University Hospital of Frankfurt, Theodor-Stern-Kai 7, D-60590 Frankfurt, Germany
[d] Department of Diagnostic and Interventional Radiology, University Hospital of Frankfurt, Theodor-Stern-Kai 7, 60590 Frankfurt, Germany
[e] Institute of Anatomy 2, University Hospital of Frankfurt, Theodor-Stern-Kai 7, D-60590 Frankfurt, Germany
[f] Institute for Inorganic and Analytic Chemistry, Goethe-University of Frankfurt, Max-von-Laue-Straße 7, D-60438 Frankfurt, Germany
[g] Nanosystem Ltd., 115193 Moscow, Russia

ARTICLE INFO

Article history:
Received 29 July 2014
Accepted 23 November 2014
Available online 10 December 2014

Keywords:
MRI
HCC
Macrophages
Gadolinium
Nanoparticle
Targeting

ABSTRACT

Nanoparticle (NP)-based contrast agents that enable high resolution anatomic T1-weighted magnetic resonance imaging (MRI) offer the prospect of improving differential diagnosis of liver tumors such as hepatocellular carcinoma (HCC). In the present study, we investigated the possibility of employing novel non-toxic human serum albumin nanoparticles conjugated with Gd-DTPA and rhodamine 123 (Gd-Rho-HSA-NPs) for the detection of HCC by T1-weighted MRI. In addition, the influence of surface coating of the NPs with poloxamine 908, which alters the absorptive behavior of NPs and changes their distribution between the liver and tumor was examined. MRI of transgenic mice with endogenously formed HCCs following intravenous injection of Gd-Rho-HSA-NPs revealed a strong negative contrast of the tumors. Contrasting of the HCCs by NP-enhanced MRI required less Gd as compared to gadolinium-ethoxybenzyl-diethylenetriaminepentaacetic acid-enhanced MRI, which currently provides the most sensitive detection of HCC in patients. Immunohistochemical analyses revealed that the Gd-Rho-HSA-NPs were localized to macrophages, which were – similar to HCC in patients – fewer in number in HCC as compared to the liver tissue, which is in agreement with the negative contrasting of HCC in Gd-Rho-HSA-NP-enhanced MRI. Poloxamine-coated NPs showed lower accumulation in the tumor macrophages and caused a longer lasting enhancement of the MRI signal. These data indicate that Gd-Rho-HSA-NPs enable sensitive detection of HCC by T1-weighted MRI in mice with endogenous HCC through their uptake by macrophages. Poloxamine coating of the NPs delayed the tumor localization of the NPs.

1. Introduction

Hepatocellular carcinoma (HCC) is the fifth most common neoplasm in the world and third most common cause of cancer-related mortality [1]. In the majority of cases it forms in the chronically inflamed and cirrhotic liver. The detection of malignant tumors such as HCC at an early stage is crucial because curative treatment options, such as surgical resection are not applicable in advanced stages of HCC [2]. Therefore, patients with chronic hepatitis, which are at high risk to develop HCC, are subject of HCC surveillance by ultrasound. Suspicious lesions are further examined by computed tomography or magnetic resonance imaging (MRI). Currently, the majority of HCCs are still diagnosed at late stages, when curative therapeutic options are not applicable any more.

Dynamic MRI enhanced by liver-specific Gd chelate contrast media such as gadolinium-ethoxybenzyl-diethylenetriaminepentaacetic acid (Gd-EOB-DTPA) currently give the best results to detect HCC radiologically [3,4]. However, the differential diagnosis of liver lesions, in particular of small HCCs (less than 1.5 cm diameter) in the cirrhotic liver, remains challenging, as the imaging often does not show the typical characteristics of HCCs. An earlier diagnosis would increase the portion of HCC patients eligible for curative treatments. Therefore, there is still a strong clinical need to improve the methods to characterize liver lesions by MRI.

* Corresponding author.
E-mail address: piiper@med.uni-frankfurt.de (A. Piiper).
[1] Equal contribution.

http://dx.doi.org/10.1016/j.jconrel.2014.11.023
0168-3659/

Nanoparticle (NP)-based contrast media offer the prospect of tumor detection by different modes than the currently used low molecular weight contrast media. Long circulating NPs may passively accumulate in tumor tissue by the enhanced penetration and retention (EPR) effect [5]. Moreover, the properties of NPs can be manipulated by alterations of the particle size, surface coating and conjugation with ligands to enable tissue-specific targeting [6,7]. These approaches require avoidance of the uptake of the NPs by the macrophages of the reticuloendothelial system (RES), mainly localized in the liver. On the other hand, the rapid uptake of NPs by macrophages can be taken as an advantage to visualize liver tumors (primary liver tumors and metastases), because the liver tissue contains higher amounts of macrophages than malignant liver tumors [8]. Indeed, superparamagnetic iron oxide nanoparticles (SPIONs), which shorten T2 relaxation and thereby act as negative contrast agents, are the only NP-based MRI contrast agent that had entered clinical routine. A critical drawback of SPION-enhanced T2-weighted MRI is that it generates signal voids that are often confounded by the presence of artifacts due to hemorrhage, air, and partial-volume effects. Signal loss in T2-weighted MRI is particularly compromised in the cirrhotic liver [9], in which the majority of HCC occurs. In contrast, Gd chelates enhance T1 relaxation, a signal-increasing imaging effect providing anatomic imaging with high spatial resolution. The bright T1 signal can clearly be distinguished from other biological or pathogenic conditions.

Recently, we have developed non-toxic human serum albumin (HSA) NPs conjugated with Gd-DTPA as well as with the fluorescent dye rhodamine 123 (Gd-Rho-HSA-NPs) [10]. These particles can be detected by MRI in vivo as well as in tissue homogenates or tissue slices by their fluorescence. The objective of the present study was the investigation of these Gd-Rho-HSA-NPs as novel contrast agents to detect HCC by T1-weighted MRI in mice with endogenously formed HCCs. In addition, the influence of surface modification of the NPs on the MRI signal by their coating with poloxamine 908, which can reduce RES uptake [11–14] and may alter the distribution of intravenously injected NPs between the HCC and liver tissue, was examined.

2. Materials and methods

2.1. Materials

Human serum albumin (HSA, fraction V, Batch 028 K7550), $GdCl_3$ and diethylenetriaminepentaacetic acid dianhydride (DTPAa) were purchased from Sigma (Steinheim, Germany), poloxamine 908 (25,000 g/mol) was obtained from BASF (Ludwigshafen, Germany). Other chemicals were of analytical grade and used as received.

2.2. Synthesis and characterization of the Gd-Rho-HSA-NPs

The preparation of HSA-NPs and the covalent attachment of Gd-DTPA and of rhodamine 123 were carried out as described recently [10]. Briefly, an amount of 5 mg DTPAa was added to 1 ml HSA-NPs, adjusted pH to 9.2, and was incubated at room temperature for 3 h under constant agitation. 20 μl 94.8 mM $GdCl_3$ was then added into HSA-DTPA and stirred at 21 °C for 30 min. The HSA-(Gd-DTPA) was subjected to dialysis against deionized water to remove excess Gd. Rhodamine 123 was covalently bound to Gd-DTPA-HSA using 1-ethyl-3-(3-dimethylaminopropyl) carbodiimide as a cross linker to produce rhodamine 123 labeled Gd-DTPA-HSA- or Gd-DTPA-Rho-HSA-NP. The mixture was incubated at room temperature for 3 h, purified by centrifugation and redispersion in 1 ml water to obtain Gd-Rho-HSA-NP.

2.3. Coating Gd-Rho-HSA NP with poloxamine 908

The NPs were mixed with an appropriate amount of 1% (w/v) solution of poloxamine 908 to obtain a final surfactant concentration of 0.5% (w/v). The NP suspensions were incubated overnight under constant agitation (550 rpm at room temperature). The modified NPs were washed by centrifugation (16,100 *g*, 8 min) to remove the excess surfactant and redispersed to the original volume in water.

2.4. Particle characterization

The mean diameter, zeta-potential and polydispersity of the resulting NPs were characterized using a Zetasizer 3000 (Malvern Instruments, Malvern, UK) as described recently [10]. The Gd(III) content of the NPs was determined by total reflection X-ray fluorescence (TXRF) (S2 Picofox, Bruker, Germany) [15,16]. The NP content in the suspension was determined by gravimetry [17].

The morphology of the NPs was examined by scanning electron microscope technique (Hitachi, S 4500 SEM). Samples were prepared by suspending the NPs in Milli-Q water, allowed to dry over 6 h at room temperature, and then sputtered with gold one to two times for 60 s. Subsequently, electron microscopy was performed using an accelerating voltage of 15–20 kV and secondary electron detection mode. The images were digitally photographed with program Digital Image Processing System 2.6.

For evaluation of the in vitro release of Gd(III) from the NPs, Gd-Rho-HSA NPs (4 mg) were placed into 2 ml of Milli-Q water, PBS pH 7.4, PBS pH 5.0 or 10% (v/v) human plasma in PBS. Each suspension was incubated at 37 °C under constant shaking. At different time points, aliquots of 200 μl were removed, centrifuged for 4 min at 8000 × *g*, and the supernatants were assayed for Gd(III) content by the TXRF method [15,16]. The pellets were resuspended with 200 ml of fresh medium and returned to the original suspensions.

2.5. In vitro MRI of the paramagnetic properties of the NPs

To determine the paramagnetic properties of Gd-Rho-HSA-NP and poloxamine-coated Gd-Rho-HSA-NPs, MRI was performed using a 3.0-T scanner (Siemens Magnetom Trio, Siemens Medical Solutions, Erlangen, Germany). The measurement conditions were T1-weighted 3D gradient echo sequences (fast low-angle shot) with the following parameters: TE = 3.31 ms, TR = 8.67 ms, field of view = 100 × 78 mm, matrix acquisition = 640 × 480, slice thickness = 0.3 mm, flip angle = 16°, fat suppression = fat saturated, and bandwidth = 180 Hz/Px.

2.6. Cellular toxicity assay

The cell viability was evaluated by a standard 3-(4,5-dimethylthiazol-2-yl)-2,5-diphenyltetrazolium bromide (MTT) assay [18]. HepG2 cells [18] were cultured in Dulbecco's Modified Eagle's Medium (DMEM) supplemented with 10% fetal bovine serum (FBS), streptomycin at 100 mg/ml and penicillin at 100 U/ml at 37 °C in a humidified atmosphere containing 5% CO_2. The HepG2 cells were placed into a 96-well plate at a density of 5×10^4 cells/ml. After 24 h of pre-incubation, the cells were further incubated for 48 and 72 h in fresh culture media containing plain HSA-NP, HSA-Gd-Rho-NP or po(HSA-Gd-Rho)-NP as 1% (w/v) poloxamine at six concentrations (16, 80, 160, 200, 320 and 640 μg/ml). Cells were then washed twice with phosphate-buffered saline (PBS) to remove excess particles. Cells incubated in the absence of NPs were used as control. Subsequently, culture medium (100 μl/well) supplemented with MTT solution (5 mg/ml, 10 μl/well) was added, followed by further incubation for 2 h. The supernatant was aspirated and 100 μl MTT lysis solution [18] was added into each well. The absorbance of cell suspension was determined at 529 nm by a microplate reader (Model 680, Bio-Rad, Hercules, CA). The percentage of viable cells was calculated by comparing absorbance of treated cells against the untreated cells (controls). Each experiment was repeated three times.

2.7. Toxicity of the NPs in mice

To investigate the toxicity of the NPs in vivo, mice were injected with PBS, Gd-Rho-HSA-NPs or po(Gd-Rho-HSA-NPs). Forty-eight hours later,

blood was drawn from the mice. Sera prepared from the blood samples were examined for C-reactive protein (CRP) content by a mouse C-reactive protein/CRP Quantikine ELISA Kit (R&D Systems, Minneapolis, MN) and a 2104 EnVision plate reader (PerkinElmer Life Sciences, Boston, MA). Blood samples were additionally analyzed for differential blood cell count using a Scil Vet ABC Analyzer (Scil Animal Care Company, Viernheim, Germany).

2.8. Isolation of peritoneal macrophages

Peritoneal macrophages were isolated from healthy mice as described [19]. The peritoneal cells were collected by washing the peritoneal cavity with 10 ml cold PBS and centrifuged at 300 ×*g* for 10 min. The collected cells were resuspended in ice cold DMEM containing 10% heat inactivated FBS and washed with the same medium. The cells were counted using a hemocytometer and cultured at a density of 2×10^6 cells/ml at 37 °C in a humidified atmosphere containing 5% CO_2.

2.9. Uptake of NPs by mouse peritoneal macrophages

For the determination of the cellular uptake of the NPs by peritoneal macrophages by flow cytometry, the cells were seeded in 24-well plates at a cell density of $1.5–2 \times 10^6$ cells per well and left to attach for 2 h. Thereafter, non-adherent cells were discarded. After cultivation for 24 h, 100, 200, and 400 μg/ml of Gd-Rho-HSA NP or poloxamine-coated Gd-Rho-HSA-NP (containing 0.5% [w/v] poloxamine 908) were added. After another hour the cells were harvested and analyzed by flow cytometry using a FACSCalibur (Becton Dickinson, Franklin Lakes, NJ). Cells incubated without NPs were used as control.

For imaging of cellular uptake of the NPs, the peritoneal macrophages were cultivated at a density of 1×10^5 cells per well in a LabTek chambered coverglass system (Thermo Fischer Scientific, Waltham, MA), allowed to attach for 2 h before discarding non-adherent cells, and cultured for 24 h. The NPs were added at a concentration of 100 μg/ml. After incubation for different time periods, the cells were washed three times and then fixed in PBS containing 4% aqueous paraformaldehyde for 10 min. A rabbit polyclonal anti-early endosomal marker (EEA1) antibody (Abcam, Cambridge, MA) was used as primary antibody, a goat anti-rabbit IgG (Chromeo™ 488) (Abcam) as secondary antibody. Nuclei were stained using Hoechst 33342 (Sigma-Aldrich, St. Louis, MO). The stained cells were then observed by confocal laser scanning microscopy (CLSM) (Olympus, FV1000, Tokyo, Japan).

2.10. MRI of TGFα/c-myc mice

The animal experiments were approved by the governmental committee (F34/07). The study protocols comply with the guidelines for animal experiments. Male transforming growth factor (TGF)α/c-myc bitransgenic mice were produced by crossing homozygous metallothionein/TGFα [20] and Alb/c-myc [21] single transgenic mice in CD13B6CBA background as described. Directly after weaning, the mice received $ZnCl_2$ to induce expression of TGFα and thereby accelerate hepatocarcinogenesis. 20–35 weeks after beginning of the zinc-induction, the animals were subjected to Gd-EOB-DTPA (0.03 mmol/kg, Primovist®, Bayer-Schering, Berlin, Germany) enhanced MRI. Approximately one week later, the mice were narcotized followed by the basal MRI and intravenous injection of 4 mg/ml of NPs (containing 0.01 mmol Gd/kg body weight), immediately followed by MRI (15 min after contrast agent injection). Subsequent MRIs were performed 3 or 24 h after the injection of the contrast agents. Imaging scans were performed using a 3 Tesla scanner (Siemens Magnetom Trio, Siemens Medical Solutions, Erlangen, Germany) as described recently [18,22]. Quantitative analyses of the MRI data were carried out as described recently [22].

2.11. Biodistribution of the NPs

NPs were administered intravenously into the mice and tissue accumulation of the NPs was detected at 15 and 30 min (3 mice for each NP). TGFα/c-myc mice with HCC were anesthetized. The mice then received 4 mg/ml of NPs via intravenous injection (0.01 mmol Gd/kg b. w.). At 15 and 30 min after the injection, blood samples were taken, the mice were sacrificed, and the organs were collected. The organs were weighed and homogenized until no solid tissue was visible. The tissue samples from non-treated mice were used as controls. To determine the content of rhodamine 123 attached to the NP, the tissue samples were analyzed for fluorescence intensity at 485/520 nm using a FLUOSTAR galaxy (BMG LabTechnologies GmbH, Offenburg, Germany). The percent injected dose per gram of tissue (%ID/g) was calculated to represent the retention of NPs in organs and tissues.

2.12. Histological analysis of the localization of the NPs in the liver and tumor tissue

TGFα/c-myc mice with HCC were intravenously injected with 4 mg/ml of NPs at a dose of 0.01 mmol Gd/kg. Fifteen or 30 min later the mice were sacrificed and the liver and tumor tissues were fixed with 4% paraformaldehyde for 24 h. Samples from untreated mice were used as controls. Ten micrometer-cryosections were prepared and were incubated with rat anti-mouse CD68 (1:25 dilution, Biolegend, San Diego, CA) in PBS containing 2% bovine serum albumin overnight at 4 °C. After washing with PBS, the sections were incubated with Alexa Fluor 633 conjugated goat anti-rat antibody (1:200 dilution, Invitrogen, Carlsbad, CA). Untreated sections without any antibody were used as negative controls. The stained sections were then examined by CLSM.

2.13. Statistical analysis

All experiments were performed at least three times on independent occasions. Data were reported as means ± standard deviation (SD) from at least three independent experiments. The statistical analysis was performed using SigmaPlot 11.0 (Systat Software, San Jose, CA) by one-way analysis of variance (ANOVA) using the Student–Newman–Keuls test. P values < 0.05 were considered to be significant.

3. Results

3.1. Characterization of Gd-Rho-HSA-NPs

HSA-NPs were prepared and conjugated with rhodamine 123 and Gd-DTPA as described recently [10]. Scanning electron microscopy and photon correlation spectroscopy of the NPs revealed a uniform size distribution with a mean diameter of 210 ± 7 nm (mean ± SD) for unmodified NPs and 233 ± 8 nm for Gd-Rho-HSA-NPs, and a polydispersity of 0.014 ± 0.010 and 0.0125 ± 0.021 for unmodified and Gd-Rho-HSA-modified NPs, respectively (means ± SD, Fig. 1 and Table 1). The Gd content of the Gd-Rho-HSA-NPs was 8.7 ± 1.1 mg/g NP and the zeta potential −35.8 ± 6.4 mV (means ± SD, Table 1). The paramagnetic properties of the NPs were confirmed by in vitro MRI. Exposure of HepG2 cells to HSA-NPs or Gd-Rho-HSA-NPs for 48 or 72 h followed by a MTT assay revealed no significant effect of the NPs on the viability of HepG2 cells (Supplementary Fig. 1).

To investigate proinflammatory effects of the NPs, the NPs were injected into mice. After 48 h blood was collected from the mice and was analyzed for white blood cell counts and the levels of CRP, an acute phase protein. There were no significant changes due to the injected NPs (Supplementary Fig. 2), supporting the assumption that these NPs were well tolerated in vivo.

As an increased risk of Gd(III) leakage by covalent binding of Gd-chelates to macromolecular systems has been reported [23], we examined the Gd(III) release from the NPs in human plasma, PBS or water

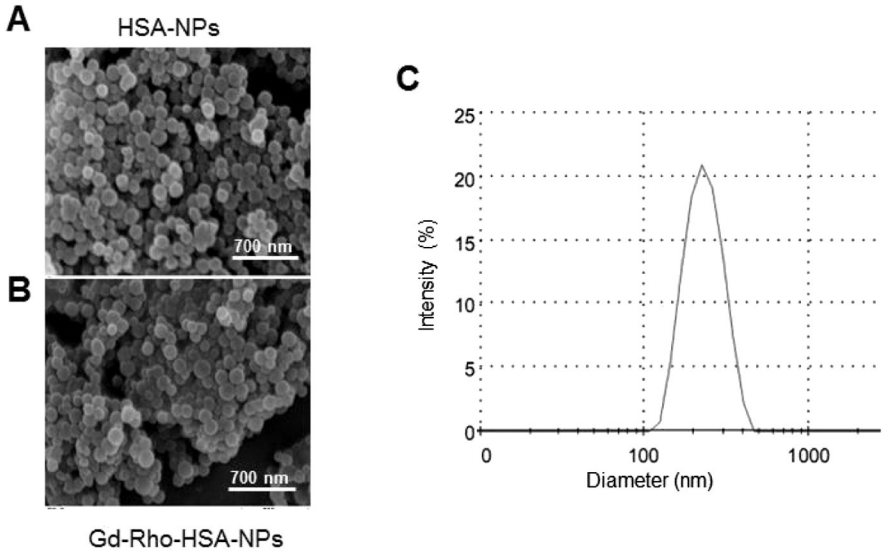

Fig. 1. Scanning electron microscope images of the NPs. (A) Unmodified HSA-NPs, (B) Gd-Rho-HSA-NPs, and (C) hydrodynamic diameter distribution of Gd-Rho-HSA-NPs as determined by photon correlation spectroscopy in water.

by the TXRF method, which detects both complexed and non-complexed NPs. As shown in Fig. 2, the NPs showed high stability, loosing only a small portion of Gd(III) during their incubation in the different media.

The absorptive behavior of the NPs governing their uptake by macrophages and thus circulation half-life can be altered by surface modification [13]. Coating of NPs with poloxamine 908 reduces the uptake of colloidal carriers [14], resulting in a prolongation of their circulation half-life, which may lead to a different distribution of the NPs between the liver and HCC. Poloxamine coating of Gd-Rho-HSA-NPs conferred a positive zeta potential to the NPs, which showed otherwise similar physicochemical properties as the non-coated NPs and no significant toxicity on cultured HepG2 cells or on the white blood cell (WBC) counts and CRP levels in mice (Table 1, Supplementary Figs. 1 and 2). Incubation of isolated mouse peritoneal macrophages with different amounts of poloxamine-coated and uncoated Gd-Rho-HSA-NPs and analyses of the uptake of the NPs by fluorescence activated cell sorting (FACS) as well as CLSM revealed a rapid and efficient uptake of the non-coated NPs by the macrophages (Fig. 3). Poloxamine coating reduced the uptake of the NPs by the macrophages at lower NP concentrations (Fig. 3), indicating that poloxamine coating conferred stealth properties to the Gd-Rho-HSA-NPs.

3.2. Imaging of HCC by Gd-Rho-HSA-NP-enhanced MRI in TGFα/c-myc mice

To investigate if the HCCs can be detected by Gd-Rho-HSA-NP-enhanced MRI, we used TGFα/c-myc bitransgenic mice, which develop HCCs endogenously within relatively short time [18,21]. The HCCs in the livers of these mice were first detected by Gd-EOB-DTPA (0.03 mmol Gd/kg)-enhanced MRI, which is highly sensitive to image HCCs in this mouse model (Supplementary Fig. 3) [18]. Gd-Rho-HSA-NPs (containing 0.01 mmol Gd/kg body weight) and additional MRIs directly following the injection of the NPs (15 min) and 3 or 24 h after the injection of the NPs. Signal enhancement in both the liver and tumor tissue was highest at 15 min after injection of the NPs and declined subsequently (Fig. 4A and B). The stronger increase of the signal intensity in the liver as compared to the tumor resulted in negatively contrasted HCCs in the livers. The contrast-to-noise ratio (CNR) was maximal in the MRI performed directly following the injection of the NPs (Fig. 4C). NPs lacking Gd-DTPA did not contrast HCCs, and Gd-HSA-NPs failed to produce contrasting in non-induced 16 weeks old TGFα/c-myc mice, in which HCC had not yet been developed.

When poloxamine-coated NPs were used instead of non-coated NPs, the contrasting of the HCCs was similar (Fig. 4D–F), but the signal enhancement in both the liver and tumor was more prolonged as compared to the MRI with the non-coated NPs (Fig. 4).

Next we compared the ability of Gd-Rho-HSA-NPs to enhance MRI signal intensity in the liver and tumor tissue in the transgenic HCC mouse model with that of an equal amount of Gd-EOB-DTPA (containing 0.01 mmol Gd-DTPA/kg body weight), the current gold standard to detect HCC by MRI in patients. As illustrated in Fig. 5, the increase in CNR in the NP-injected mice was considerably higher as compared to animals injected with Gd-EOB-DTPA, indicating that lower amounts of Gd-DTPA were required to detect HCC by NP-enhanced MRI as compared to Gd-EOB-DTPA-enhanced MRI.

3.3. Intravenously injected Gd-Rho-HSA-NPs localized to macrophages in the liver

To support the observation that intravenously injected Gd-Rho-HSA-NPs primarily localize to the liver, presumably due to their uptake into liver macrophages, we measured the distribution of Gd-Rho-HSA-NPs in different tissues upon their intravenous injection into HCC mice. The NP-associated fluorescence reached the highest values in the liver (Fig. 6). Significant NP uptake was also observed in the tumor, heart, pancreas, and lung, but not in the brain or spleen. These data support the results obtained in MRI that the intravenously administered Gd-Rho-HSA-NPs mainly accumulated in the liver, whereas the amount of

Table 1
Physicochemical parameters of unmodified and poloxamine-modified HSA-NPs in distilled water ($n \geq 3$).

	Particle size [nm]	Polydispersity	Zeta potential [mV]	Particle content [mg/ml]	Gd [mg/l]	mg Gd per g NP
Unmodified NSA-NP	211 ± 7	0.014 ± 0.010	−41.8 ± 4.1	19.1 ± 0.9		
Gd-Rho-HSA-NPs	233 ± 8	0.026 ± 0.021	−35.8 ± 6.4	16.8 ± 0.8	149.6 ± 12.2	8.7 ± 1.1
po(Gd-Rho-HSA)-NPs	244 ± 22	0.054 ± 0.046	25.6 ± 14.1	19.4 ± 2.3	163.7 ± 30.1	7.8 ± 2.0

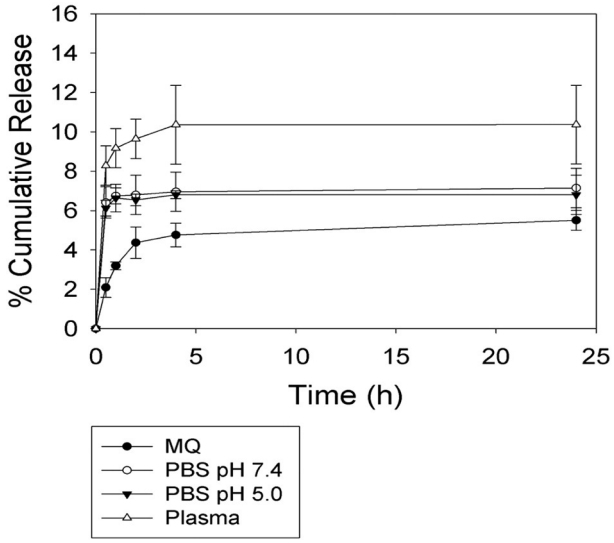

Fig. 2. Release profile of Gd(III) from Gd-Rho-HSA NPs in different media. The NPs (2 mg/ml) were incubated in Milli-Q water or PBS pH 7.4, PBS pH 5.0 or plasma at 37 °C. Data were given as mean ± SD (n = 3).

NPs that reached the other organs and the HCCs was considerably lower, resulting in negative contrasting of the HCCs in the liver by Gd-Rho-HSA-NP-enhanced MRI.

In general, the accumulation of the NPs in the liver occurs mainly due to their efficient uptake by the liver macrophages (Kupffer cells). It is also known that the normal liver shows a higher density of macrophages as compared to malignant liver tumors [8]. To investigate the distribution of the NPs in Kupffer cells and tumor-associated macrophages, mice with Gd-EOB-DTPA-verified HCCs were injected intravenously with Gd-Rho-HSA-NPs. Fifteen or 30 min later the mice were sacrificed and the livers were excised, fixed, and slices of the livers were stained with anti-CD68, a marker for macrophages, and examined for the localization of the NPs within the liver and tumor tissue by CLSM. As illustrated in Fig. 7B and C, the fluorescence of the NPs was more intensive in the liver as compared to the HCCs. No red fluorescence was found in livers from animals not injected with NPs (Fig. 7A). The number of CD68-positive cells in the liver was much higher than in the tumor tissue, and the majority of the fluorescence of the NPs co-localized with the macrophages in both the liver and tumor tissue. Determination of the percentage of CD68-positive cells that contained fluorescent NPs revealed a decreased amount of Gd-Rho-HSA-NPs in the tumor macrophages as compared to the Kupffer cells (Fig. 7D).

Similar to the effect of poloxamine coating on the uptake of the NPs by peritoneal macrophages in vitro, HCC mice injected intravenously with poloxamine-coated Gd-Rho-HSA-NPs showed reduced localization to NPs in the tumor tissue. The determination of the portion of CD68 positive cells containing NP-associated fluorescence revealed a reduced portion of CD68 positive cells containing NP-associated fluorescence in animals injected with poloxamine-coated NPs as compared to mice injected with non-coated NPs in the tumors and livers (Fig. 7D). Together, these data indicate that the intravenously injected Gd-Rho-HSA-NPs were rapidly taken up by the macrophages in the liver as well as in the tumor, producing negatively contrasted HCCs in MRI probably due to the lower density of macrophages in the HCCs as compared to the surrounding liver tissue. This can be modified by poloxamine coating of the NPs.

4. Discussion and conclusions

NP-based MRI contrast media may provide additional tools for the detection and differential diagnosis of liver lesions, because they show different pharmacokinetics than the currently used small molecule contrast media. Moreover, their properties can be tailored according to the needs by various modifications. We recently produced and characterized

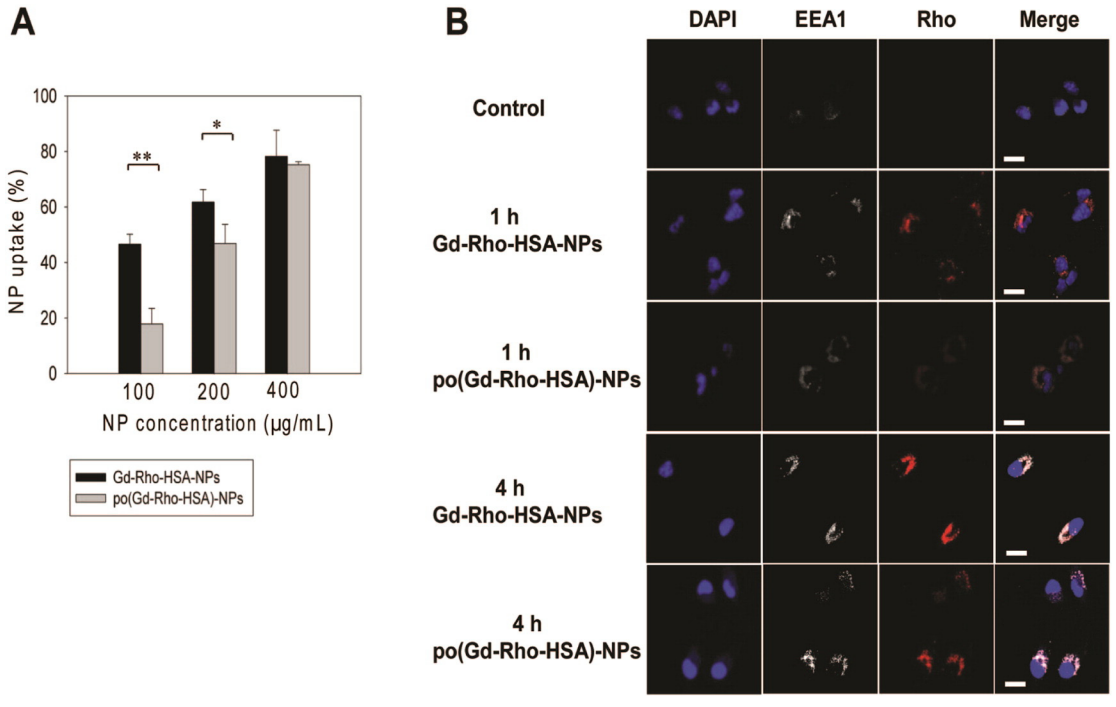

Fig. 3. Reduced uptake of poloxamine-coated NPs as compared to non-coated NPs by mouse peritoneal macrophages. (A) Uptake of Gd-Rho-HSA-NPs or poloxamine-coated Gd-Rho-HSA-NPs (po(Gd-Rho-HSA)-NPs) by peritoneal macrophages after 1 h of incubation at different NP concentrations (100, 200 and 400 μg/ml) at 37 °C. The measurement was performed by FACS analysis (means ± SD; n = 3). $^{*}P < 0.05$; $^{**}P < 0.01$. (B) CLSM images of peritoneal macrophages incubated with or without Gd-Rho-HSA- or poloxamine-coated Gd-Rho-HSA-NPs (po(Gd-Rho-HSA)-NPs) (200 μg/ml of each NP formulation) for 1 h at 37 °C. The images were obtained using three channels shown in each column: blue for cell nuclei, white for endosomes, red for NPs. The merged images display the overlay of all fluorescence channels. Endosomes (white) were stained with rabbit polyclonal anti-EEA1 antibody to facilitate the visualization of the intracellular uptake of the NPs, and cell nuclei (blue) were stained with Hoechst 33342. Scale bar = 10 μm.

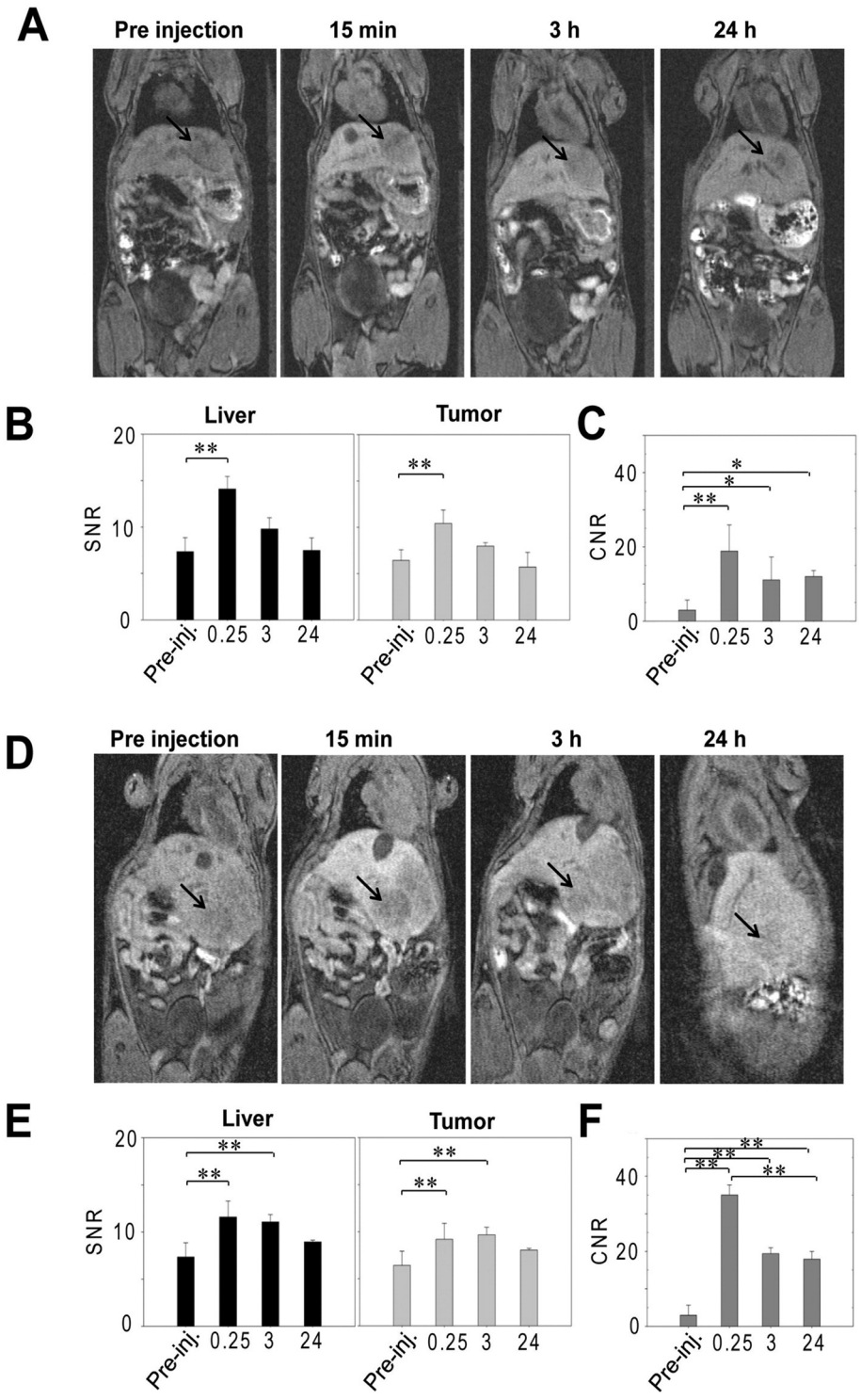

Fig. 4. Imaging of HCC by uncoated and poloxamine-coated Gd-Rho-HSA-NPs in TGFα/c-myc mice. Representative time courses of MRI of HCC mice injected with Gd-Rho-HSA-NPs (A–C) or poloxamine-coated Gd-Rho-HSA-NPs (po(Gd-Rho-HSA)-NPs) (D–F). The animals were scanned immediately before (pre-injection) and 15 min, 3 h or 24 h after the injection of the NPs. The layers in the images for 3 and 24 h are not identical, showing different localization of organs and appearance of HCC as a result of different animal used. (B, E) Comparison of the signal to noise ratio (SNR) of the liver and tumor in Gd-Rho-HSA-NP- (B) and po(Gd-Rho-HSA)-NP-injected TGFα/c-myc mice (E) at the indicated time after the injection of the NPs. The NPs were administered into the mice at a Gd dose of 0.01 mmol/kg. (C, F) Comparison of the contrast to noise ratio (CNR) of Gd-Rho-HSA-NP- (C) and po(Gd-Rho-HSA)-NP-injected mice (F). Quantification of the MRI signal intensity of the HCCs was performed by subtracting the signal intensity before (pre-injection) and after administration of each NP at the Gd dose of 0.01 mmol/kg for all measurements. The data are presented as means ± SD from n ≥ 3 mice/group. There was a significant difference as shown (**$P < 0.01$). Arrows indicate the locations of HCC.

non-toxic biodegradable HSA-NPs conjugated with Gd-DTPA and rhodamine 123 with high stability in serum and PBS. These NPs can be detected by MRI in vivo as well as by their fluorescence in tissue homogenates or tissue slices [10]. The latter is important for exact localization of the NPs in the tissues, which facilitates their further development as contrast agents. Using these dually labeled Gd- and rhodamine 123-conjugated NPs consisting of a HSA core, we show here that Gd-labeled NPs effectively contrasted HCCs in MRI in a transgenic mouse model

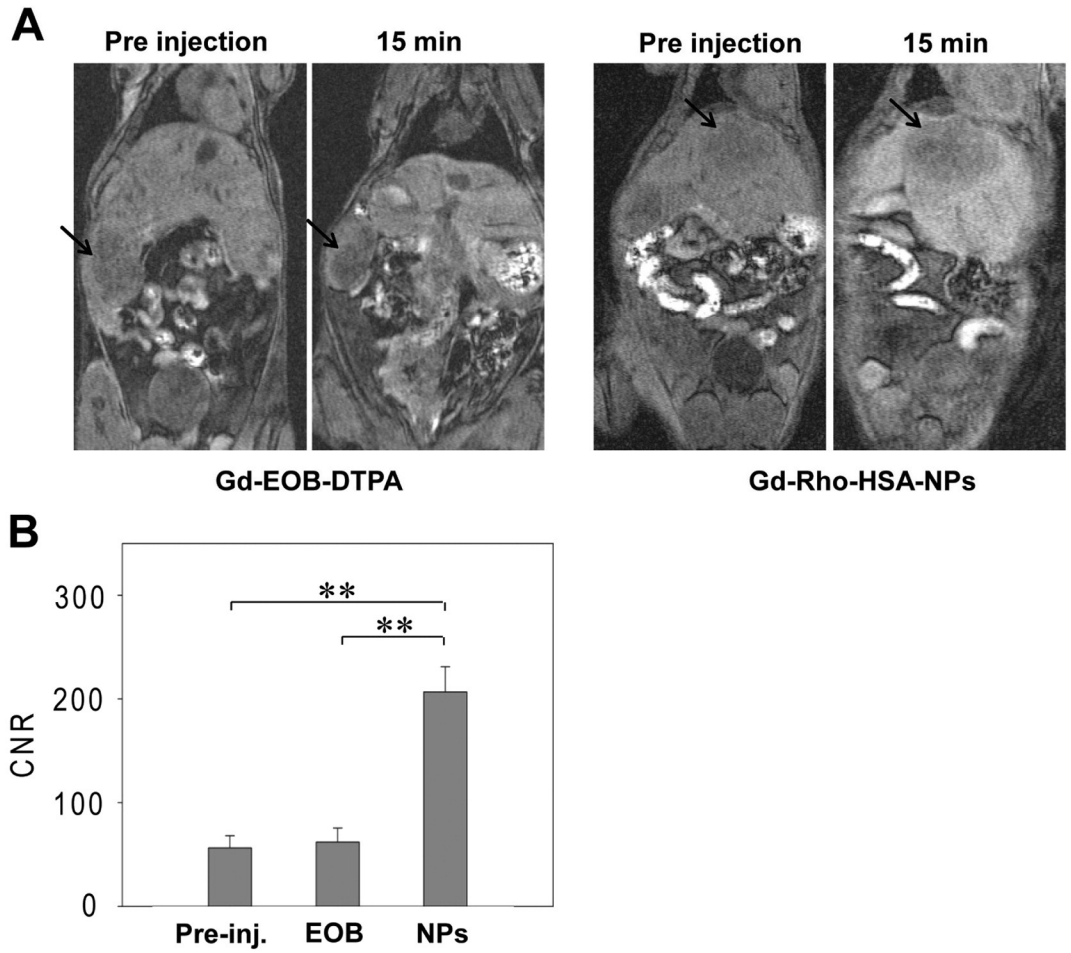

Fig. 5. Comparison of the sensitivity of Gd-EOB-DTPA- and Gd-Rho-HSA-NP-enhanced MRI to detect HCC. Mice with HCC, as revealed by MRI with an optimal dose of Gd-EOB-DTPA (0.03 mmol/kg) one week before, were subjected to a basal MRI followed by injection of Gd-Rho-HSA-NPs or Gd-EOB-DTPA (0.01 mmol/kg) and another MRI. (A) Representative MR images. Arrows indicate the locations of HCC. (B) Quantitative analysis of CNR of livers and tumors. The data are displayed as means ± SD from n = 3 mice/group. Asterisks indicate significant differences; $^{**}P < 0.01$.

with endogenously formed HCCs, i.e. in a patient-relevant HCC mouse model. As imaging of HCCs in the liver by Gd-NP-enhanced MRI has not yet been achieved in other studies, this study provides the first evidence that Gd-conjugated NPs can contrast HCCs in the liver.

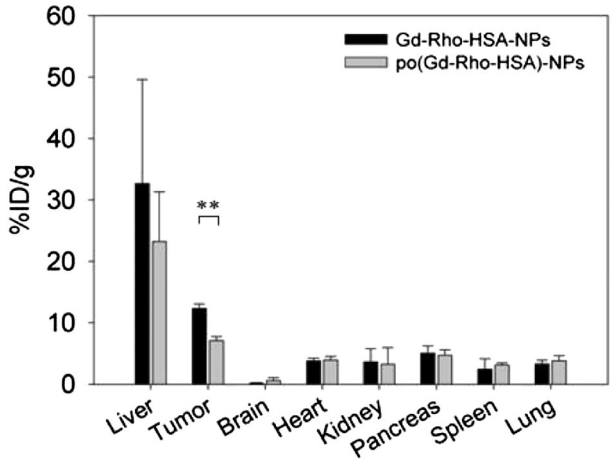

Fig. 6. Tissue distribution of NPs in HCC mice 15 min after intravenous injection of the NPs. Results are reported as % injection dose per gram of organ (%ID/g). Data are presented as means ± SD from n = 3 mice/group ($^{**}P < 0.01$).

The covalent binding of DTPA to the NPs in principle could decrease the stability of the Gd(III) complex [23], leading to the release of the toxic uncomplexed Gd(III). However, we found no significant cellular toxicity or signs of inflammation after NP administration in mice. Moreover, as more Gd was required to increase the MRI signal of the liver upon injection of Gd-EOB-DTPA as compared to Gd-Rho-HSA-NPs, it is unlikely that Gd released from the NPs contributes to the contrasting of HCC in Gd-Rho-HSA-NP-enhanced MRI.

In the present study we aimed to improve the pre-existing clinically successful approach of visualization of HCC by taking advantage of the differential distribution of macrophages between the liver and malignant liver tumors and the rapid uptake of NPs by macrophages using Gd-labeled NPs that can be detected by T1-weighted MRI. This is advantageous because SPION-enhanced visualization of HCC requires T2-weighted MRI, which negatively contrasts the underlying structures providing ambiguous imaging, in particular in cirrhotic livers, which holds for the majority of HCC patients [9]. Thus, the high resolution contrast-enhanced T1-weighted MRI of liver lesions using Gd-labeled HSA-NPs described in the present study should be superior to SPION-enhanced MRI for imaging of liver lesions.

Gd-Rho-HSA-NPs caused negative contrasting of the HCCs in the liver. Immune fluorescence microscopy of tissue slices from the liver and HCC of mice injected with the NPs revealed that the majority of the NPs co-localized with CD68 positive macrophages, which were found to be fewer in HCC tissue as compared to the surrounding liver tissue in this HCC mouse model with endogenous HCCs similar to HCC

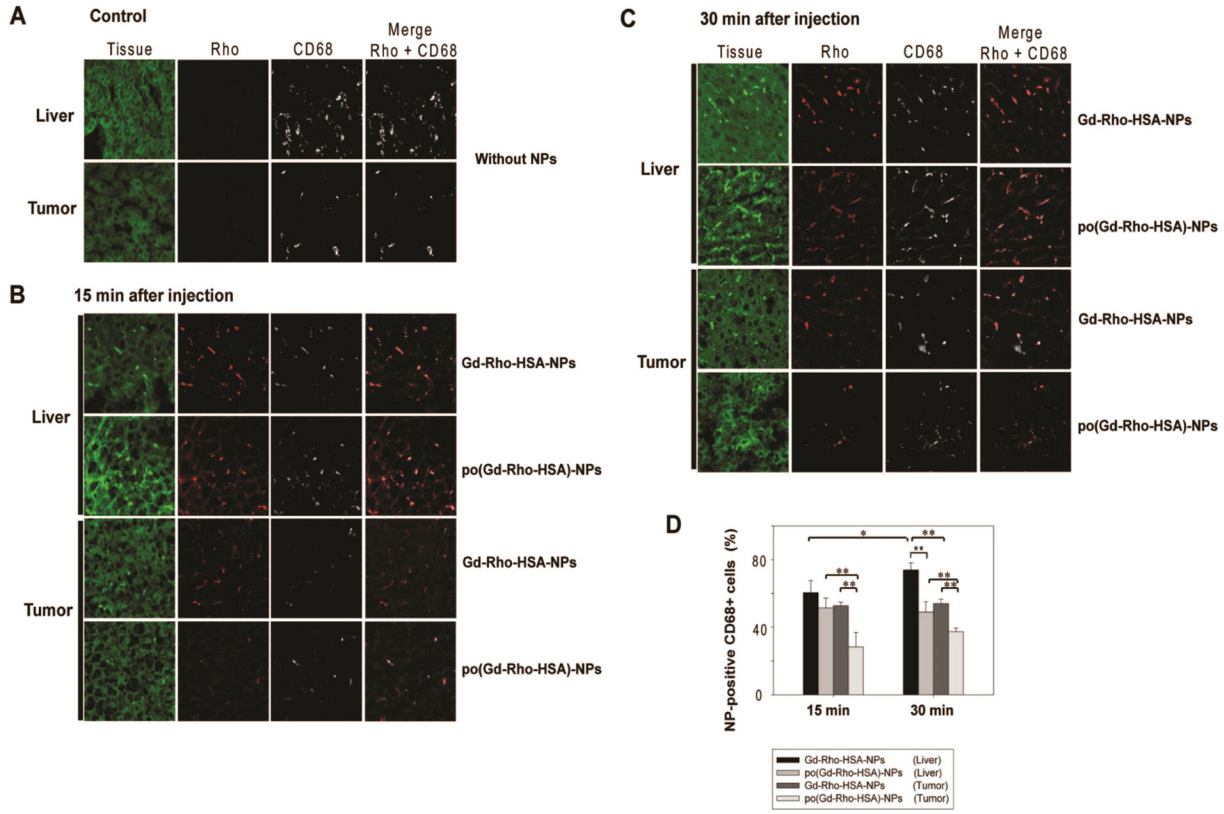

Fig. 7. Histological analysis of the localization of Gd-Rho-HSA-NPs and poloxamine-coated Gd-Rho-HSA-NPs in liver and tumor tissue sections. Representative CLSM images show the localization of the NPs in macrophages and their distribution before and 15 or 30 min after the injection of the indicated NPs. Tissue autofluorescence is shown in green for background, the fluorescence of the NPs in red, and staining of CD68 positive macrophages in white. (A) Untreated tissues; upper panel: stained liver tissue sections before injection of NPs; lower panel: stained tumor tissues. (B, C) Sections of liver and tumor tissues 15 (B) or 30 min (C) after the injection of Gd-Rho-HSA- or po(Gd-Rho-HSA)-NPs as indicated. (D) Quantitative analyses of the % co-localization of the NPs with the macrophages in the liver and tumor tissue analyzed by the software ImageJ. The data represent means ± SD (n = 3 mice/group). $^{*}P < 0.05$; $^{**}P < 0.01$.

patients. In agreement with these data, isolated peritoneal macrophages rapidly took up the NPs and biodistribution analyses revealed preferential localization of the systemically administered NPs in the liver over other organs and HCCs. Thus, the negatively contrasted HCCs in the liver in MRI can be readily explained by the rapid uptake of the intravenously administered Gd-Rho-HSA-NPs into the macrophages, which were differentially distributed between the HCC and surrounding liver tissue.

Gd-conjugated polylactic acid NPs and polyamidoamine dendrimers have been developed to specifically target the tumor cells [24,25]. This approach requires NPs that either bind strongly and specifically to the tumor cells in vivo or circulate continuously in the blood to enable penetration into the tumor due to the EPR effect. However, these requirements are difficult to fulfill. We here investigated if coating of the NPs with poloxamine to confer stealth properties to the NPs altered the distribution of the NPs between the liver and tumor. As expected, poloxamine-coated NPs showed a reduced uptake by peritoneal macrophages ex vivo. At high concentrations the uptake of the poloxamine-coated and uncoated NPs by the macrophages was similar, suggesting that this process reached the level of saturation. This phenomenon was also observed by others [26,27]. In agreement with a reduced uptake of poloxamine-coated NPs by macrophages, examination of liver slices from mice injected with poloxamine-coated and non-coated NPs revealed that the poloxamine-coated NPs showed a reduced localization in the macrophages in the liver and tumor tissue. However, poloxamine coating did not significantly alter the initial enhancement of the signal intensity in the liver and tumor tissue in Gd-Rho-HSA-NP-enhanced MRI. At present we cannot explain this minor difference between the MRI and the immunofluorescence images of the tissue slices. The visualization of the NPs in the tissue by histology and in early in vivo MRI differs in that signal enhancement in MRI is due to Gd-labeled NPs in the tissue and in the blood vessels, whereas residually circulating NPs were washed out in the histological approach, in which the animals were perfused prior to the removal of the livers. Nevertheless, our data indicate that surface modification of the NPs can alter the biodistribution of the NPs, which might be useful to tailor NP-based contrast media to the specific needs.

Our novel NP contrast agents required less Gd-DTPA to visualize the HCCs by MRI than Gd-EOB-DTPA, the currently best MRI contrast agent for the detection of HCC in patients, in the HCC mouse model. This could be due to the slower renal excretion of the macromolecular NPs as compared to free Gd chelates and might be of clinical relevance considering the reported risk of nephrotoxic effects of Gd chelate-containing contrast agents, in particular in patients with kidney dysfunction [28]. Thus, NP-based Gd-conjugated contrast media may be preferable over small molecule contrast media in patients with pre-existing kidney damage.

In principle, similar to other small molecule Gd chelate contrast media, Gd-labeled HSA-NPs may also be capable to detect HCC by its frequently encountered and typical early arterial hyperperfusion in dynamic MRI. For technical reasons, we could not perform dynamic MRI in our mouse model. However, there is no indication that Gd-HSA-NP-based contrast media may be advantageous for this purpose in comparison to the small molecule Gd containing contrast media.

In summary, the data of present study indicate that Gd-labeled HSA-NPs constitute a new non-toxic biodegradable MRI contrast agent that enables highly sensitive and high resolution detection of HCC in a mouse model with endogenous hepatocarcinogenesis, most likely by signal enhancement of the macrophages in the liver and tumor in T1-weighted MRI. The uptake of the NPs by the macrophages can be modified by surface coating of the NPs, which may be used to obtain NPs with a different diagnostic potential.

Acknowledgments

We thank Manfred Ruppel (Department of Biological Sciences, University of Frankfurt, Germany) for performing scanning electron microscopy, Snorri Thorgeirsson (Laboratory of Experimental Carcinogenesis, Center for Cancer Research, National Cancer Institute, National Institutes of Health, Bethesda, MD) for kindly providing c-myc and TGFα transgenic mice, Claudia Rittmeyer (Institute for Inorganic and Analytic Chemistry, Goethe-University of Frankfurt) for TXRF measurement, and Andreas Weigert (Institute of Biochemistry, University Hospital Frankfurt, Germany) for advice concerning staining tissue slices and valuable discussion. This work was supported by grants from the Deutsche Forschungsgemeinschaft (GRK1172) and the Medical Faculty of the University of Frankfurt (Dr. Paul und Cilli Weil-Stiftung and Heinrich und Fritz Riese-Stiftung). W. Watcharin was supported by a fellowship from Assumption University of Thailand.

Appendix A. Supplementary data

Supplementary data to this article can be found online at http://dx.doi.org/10.1016/j.jconrel.2014.11.023.

References

[1] A. Jemal, F. Bray, M.M. Center, J. Ferlay, E. Ward, D. Forman, Global cancer statistics, CA Cancer J. Clin. 61 (2011) 69–90.
[2] H.B. El-Serag, K.L. Rudolph, Hepatocellular carcinoma: epidemiology and molecular carcinogenesis, Gastroenterology 132 (2007) 2557–2576.
[3] S.S. Raman, C. Leary, D.A. Bluemke, M. Amendola, D. Sahani, J.D. McTavish, J. Brody, E. Outwater, D. Mitchell, D.H. Sheafor, J. Fidler, I.R. Francis, R.C. Semelka, K. Shamsi, S. Gschwend, D.R. Feldman, J. Breuer, United States EOB Study Group, Improved characterization of focal liver lesions with liver-specific gadoxetic acid disodium-enhanced magnetic resonance imaging: a multicenter phase 3 clinical trial, J. Comput. Assist. Tomogr. 34 (2010) 163–172.
[4] T. Ichikawa, K. Saito, N. Yoshioka, A. Tanimoto, T. Gokan, Y. Takehara, T. Kamura, T. Gabata, T. Murakami, K. Ito, S. Hirohashi, A. Nishie, Y. Saito, H. Onaya, R. Kuwatsuru, A. Morimoto, K. Ueda, M. Kurauchi, J. Breuer, Detection and characterization of focal liver lesions: a Japanese phase III, multicenter comparison between gadoxetic acid disodium-enhanced magnetic resonance imaging and contrast-enhanced computed tomography predominantly in patients with hepatocellular carcinoma and chronic liver disease, Invest. Radiol. 45 (2010) 133–141.
[5] H. Maeda, Tumor-selective delivery of macromolecular drugs via the EPR effect: background and future prospects, Bioconjug. Chem. 21 (2010) 797–802.
[6] A. Albanese, P.S. Tang, W. Chan, The effect of nanoparticle size, shape, and surface chemistry on biological systems, Annu. Rev. Biomed. Eng. 14 (2012) 1–16.
[7] S. Salmaso, P. Caliceti, Stealth properties to improve therapeutic efficacy of drug nanocarriers, J. Drug Deliv. 2013 (2013) 374252.
[8] L.H. Reddy, P. Couvreur, Nanotechnology for therapy and imaging of liver diseases, J. Hepatol. 55 (2011) 1461–1466.
[9] A. Tanimoto, S. Kuribayashi, Application of superparamagnetic iron oxide to imaging of hepatocellular carcinoma, Eur. J. Radiol. 58 (2006) 200–216.
[10] W. Watcharin, C. Schmithals, T. Pleli, V. Köberle, H. Korkusuz, F. Huebner, S. Zeuzem, H.W. Korf, T.J. Vogl, C. Rittmeyer, A. Terfort, A. Piiper, S. Gelperina, J. Kreuter, Biodegradable human serum albumin nanoparticles as contrast agents for the detection of hepatocellular carcinoma by magnetic resonance imaging, Eur. J. Pharm. Biopharm. 87 (2014) 132–141.
[11] S. Stolnik, L. Illum, S.S. Davis, Long circulating microparticulate drug carriers, Adv. Drug Deliv. Rev. 16 (1995) 195–214.
[12] L. Araujo, R. Löbenberg, J. Kreuter, Influence of the surfactant concentration on the body distribution of nanoparticles, J. Drug Target. 6 (1999) 373–385.
[13] S.M. Moghimi, A.C. Hunter, T.L. Andresen, Factors controlling nanoparticle pharmacokinetics: an integrated analysis and perspective, Annu. Rev. Pharmacol. Toxicol. 52 (2012) 481–503.
[14] L. Illum, S.S. Davis, Targeting of colloidal particles to the bone marrow, Life Sci. 40 (1987) 1553–1560.
[15] L. Telgmann, M. Holtkamp, J. Kuennemeyer, C. Gelhard, M. Hartmann, A. Klose, M. Sperling, U. Karst, Simple and rapid quantification of gadolinium in urine and blood plasma samples by means of total reflection X-ray fluorescence (TXRF), Metallomics 3 (2011) 1035–1040.
[16] R. Delfino, M. Altissimo, R.H. Menk, R. Alberti, T. Klatka, T. Frizzi, A. Longoni, M. Salomè, G. Tromba, F. Arfelli, M. Clai, L. Vaccari, V. Lorusso, C. Tiribelli, L. Pascolo, X-ray fluorescence elemental mapping and microscopy to follow hepatic disposition of a Gd-based magnetic resonance imaging contrast agent, Clin. Exp. Pharmacol. Physiol. 38 (2011) 834–845.
[17] K. Ulbrich, M. Michaelis, F. Rothweiler, T. Knobloch, P. Sithisarn, J. Cinatl, J. Kreuter, Interaction of folate-conjugated human serum albumin (HSA) nanoparticles with tumour cells, Int. J. Pharm. 406 (2011) 128–134.
[18] J. Haupenthal, V. Bihrer, H. Korkusuz, O. Kollmar, C. Schmithals, S. Kriener, K. Engels, T. Pleli, A. Benz, M. Canamero, T. Longerich, B. Kronenberger, O. Waidmann, S. Richter, T.J. Vogl, S. Zeuzem, A. Piiper, Reduced efficacy of the Plk1 inhibitor BI 2536 on the progression of hepatocellular carcinoma due to low intratumoral drug levels, Neoplasia 14 (2012) 410–419.
[19] A. Ray, B.N. Dittel, Isolation of mouse peritoneal cavity cells, J. Vis. Exp. (35) (Jan 28 2010), http://dx.doi.org/10.3791/1488 (pii: 1488).
[20] C. Jhappan, C. Stahle, R.N. Harkins, N. Fausto, G.H. Smith, G.T. Merlino, TGFα overexpression in transgenic mice induces liver neoplasia and abnormal development of the mammary gland and pancreas, Cell 61 (1990) 1137–1146.
[21] H. Murakami, N.D. Sanderson, P. Nagy, P.A. Marino, G. Merlino, S.S. Thorgeirsson, Transgenic mouse model for synergistic effects of nuclear oncogenes and growth factors in tumorigenesis: interaction of c-myc and transforming growth factor α in hepatic oncogenesis, Cancer Res. 53 (1993) 1719–1723.
[22] H. Korkusuz, K. Ulbrich, K. Welzel, K. Koeberle, W. Watcharin, U. Bahr, V. Chernikov, T. Knobloch, S. Petersen, F. Huebner, H. Ackermann, S. Gelperina, W. Kromen, R. Hammerstingl, J. Haupenthal, F. Gruenwald, J. Fiehler, S. Zeuzem, J. Kreuter, T.J. Vogl, A. Piiper, Transferrin-coated gadolinium nanoparticles as MRI contrast agent, Mol. Imaging Biol. 15 (2013) 148–154.
[23] R. Duncan, L. Izzo, Dendrimer biocompatibility and toxicity, Adv. Drug Deliv. Rev. 57 (2005) 2215–2237.
[24] Z. Cheng, D. Thorek, A. Tsourkas, Gd-conjugated dendrimer nanoclusters as a tumor-targeted T1 magnetic resonance imaging contrast agent, Angew. Chem. Int. Ed. Engl. 49 (2010) 346–350.
[25] Y. Liu, Z. Chen, C. Liu, D. Yu, Z. Lu, N. Zhang, Gadolinium-loaded polymeric nanoparticles modified with anti-VEGF as multifunctional MRI contrast agents for the diagnosis of liver cancer, Biomaterials 32 (2011) 5167–5176.
[26] J. Panyam, V. Labhasetwar, Dynamics of endocytosis and exocytosis of poly(D,L-lactide-co-glycolide) nanoparticles in vascular smooth muscle cells, Pharm. Res. 20 (2003) 212–220.
[27] J. Davda, V. Labhasetwar, Characterization of nanoparticle uptake by endothelial cells, Int. J. Pharm. 233 (2002) 51–59.
[28] H.S. Thomsen, T. Alme'n, S.K. Morcos, Members of Contrast Media Safety Committee of European Society of Urogenital Radiology (ESUR), gadolinium-containing contrast media for radiographic examinations: a position paper, Eur. Radiol. 12 (2002) 2600–2605.